PHYSICAL REVIEW A **98**, 040501(R) (2018)

Rapid Communications

Relativistic full-configuration-interaction calculations of magic wavelengths for the $2\,^3S_1 \rightarrow 2\,^1S_0$ transition of helium isotopes

Fang-Fei Wu,[1,2] San-Jiang Yang,[1,3] Yong-Hui Zhang,[1,*] Jun-Yi Zhang,[1] Hao-Xue Qiao,[3] Ting-Yun Shi,[1,4] and Li-Yan Tang[1,†]

[1] *State Key Laboratory of Magnetic Resonance and Atomic and Molecular Physics, Wuhan Institute of Physics and Mathematics, Chinese Academy of Sciences, Wuhan 430071, People's Republic of China*

[2] *University of Chinese Academy of Sciences, Beijing 100049, People's Republic of China*

[3] *Department of Physics, Wuhan University, Wuhan 430072, People's Republic of China*

[4] *Center for Cold Atom Physics, Chinese Academy of Sciences, Wuhan 430071, People's Republic of China*

(Received 30 May 2018; published 5 October 2018)

A large-scale full-configuration-interaction calculation based on the Dirac-Coulomb-Breit (DCB) Hamiltonian is performed for the $2\,^1S_0$ and $2\,^3S_1$ states of helium. The operators of the normal and specific mass shifts are directly included in the DCB framework to take the finite nuclear mass correction into account. High-accuracy energies and matrix elements involved n (the main quantum number) up to 13 are obtained from one diagonalization of Hamiltonian. The dynamic dipole polarizabilities are calculated by using the sum rule of intermediate states, and a series of magic wavelengths with QED and hyperfine effects included for the $2\,^3S_1 \rightarrow 2\,^1S_0$ transition of helium are identified. In addition, the high-order ac Stark shift determined by the dynamic hyperpolarizabilities at the magic wavelengths are also evaluated. Since the most promising magic wavelength for application in experiment is 319.8 nm, the high-accuracy magic wavelength of 319.815 3(6) nm of ^{4}He is in good agreement with the recent measurement value of 319.815 92(15) nm [R. J. Rengelink *et al.*, arXiv:1804.06693], and the present magic wavelength of 319.830 2(7) nm for ^{3}He would provide theoretical support for experimentally designing an optical dipole trap to precisely determine the nuclear charge radius of helium in the future.

DOI: 10.1103/PhysRevA.98.040501

The long-term outstanding proton radius puzzle causes great interest in recent years [1–3]. So far there has not been a satisfying explanation for the discrepancy of 5.6σ in the proton size derived from muonic hydrogen Lamb shift measurements [1,2] and the accepted CODATA value [3]. Research in this field has expanded to measurements of the $2S$-$4P$ transition energy in hydrogen [4], transition energies between circular Rydberg states in heavy-H-like ions [5], and the $1S$-$2S$ transition energy in muonic helium ions [6]. In order to help solve the proton size puzzle, the measurement of high-precision spectroscopy in helium isotopes has become an additional contribution to this field [7–12]. However, the nuclear charge radius difference determined from the $2\,^3S \rightarrow 2\,^1S$ and $2\,^3S \rightarrow 2\,^3P$ transitions of helium disagrees by 4σ [7–12]. Even combined with the recent theoretical investigations [13–15], where the higher-order recoil corrections are taken into account, the 4σ discrepancy does still exist and remains unexplained by any missed corrections in existing theoretical predictions. So this discrepancy calls for the verification of the experimental transition frequencies by independent measurements.

For the $2\,^3S \rightarrow 2\,^3P$ transition frequency of helium, recently, the frequency measurement of ^{4}He is achieved to 5.1×10^{-12} [16], which is more accurate than the early results of Refs. [11,12,17]. But it's interesting that applying the $2\,^3S \rightarrow 2\,^3P$ transition frequency of ^{3}He of Ref. [12] into Ref. [16], the resulting nuclear charge radii difference agrees well with the value derived from the $2\,^3S \rightarrow 2\,^1S$ transition [7] but differs with the measurement of the $2\,^3S \rightarrow 2\,^3P$ transition [9]. This deviation indicates that further independent measurement of the $2\,^3S \rightarrow 2\,^3P$ transition for ^{3}He is urgently needed.

For the $2\,^3S \rightarrow 2\,^1S$ transition frequency of helium, one of the main systematic uncertainties of previous measurement [7] comes from ac Stark shift. Implementation of a magic wavelength trap can solve this problem in many high-precision measurements [18,19]. Recently, Notermans *et al.* obtained the magic wavelengths of He($2\,^3S \rightarrow 2\,^1S$) with the use of available energies and Einstein A coefficients [20]. The accuracy of their values is limited by extrapolated contributions from continuums.

Since the dynamic dipole polarizability at the 319.8 nm magic wavelength is large enough to provide sufficient trap depth at reasonable laser powers while the scattering lifetime is accepted, the 319.8 nm magic wavelength is proposed to design an optical dipole trap (ODT) to eliminate the ac Stark shift [20]. In order to determine the nuclear charge radius difference with a precision comparable to the muonic helium ion, Vassen *et al.* aim to measure the $2\,^3S \rightarrow 2\,^1S$ transition with subkilohertz precision. At this level of precision, the *ab initio* calculation for the magic wavelengths of helium isotopes is required.

---

[*] yhzhang@wipm.ac.cn

[†] lytang@wipm.ac.cn

2469-9926/2018/98(4)/040501(7)

In this Rapid Communication, we improve the previous relativistic configuration interaction (RCI) method [21] by adding the mass shift (MS) operators directly into the Dirac-Coulomb-Breit (DCB) Hamiltonian. Then we perform a large-scale full-configuration-interaction calculation of the dynamic dipole polarizabilities for the $2\,^3S$ and $2\,^1S$ states of helium. QED corrections to the dynamic dipole polarizabilities are approximate by perturbation calculations. A series of magic wavelengths for the $2\,^3S_1 \rightarrow 2\,^1S_0$ transition are accurately identified according to the dynamic polarizabilities. In addition, we also carry out nonrelativistic calculations of dynamic polarizabilities and hyperpolarizabilities of helium by using the newly developed Hylleraas-B-spline method [22]. Present magic wavelengths from two different theoretical methods are in good agreement. Specifically, the accurate magic wavelengths of 319.815 3(6) nm and 319.830 2(7) nm are recommended for the $2\,^3S_1(M_J = \pm 1) \rightarrow 2\,^1S_0$ transition of ^{4}He and ^{3}He, respectively.

The DCB Hamiltonian with mass shift operator included for the two-electron atomic system is written as

$$H = \sum_{i=1}^{2}\left[c\boldsymbol{\alpha}_i \cdot \boldsymbol{p}_i + \beta m_e c^2 - \frac{Z}{r_i}\right] + \frac{1}{r_{12}} - \frac{1}{2r_{12}}[\boldsymbol{\alpha}_1 \cdot \boldsymbol{\alpha}_2 + (\boldsymbol{\alpha}_1 \cdot \hat{\boldsymbol{r}}_{12})(\boldsymbol{\alpha}_2 \cdot \hat{\boldsymbol{r}}_{12})] + H_{\text{MS}}, \tag{1}$$

where $c = 137.035\,999\,074$ is the speed of light [23], Z is the nuclear charge, β is the 4×4 Dirac matrix, $m_e = 1$ is the electron mass, $\boldsymbol{\alpha}_i$ and $\boldsymbol{p}_i$ are, respectively, the Dirac matrix and the momentum operator for the ith electron, $\hat{\boldsymbol{r}}_{12}$ is the unit vector of the electron-electron distance $\boldsymbol{r}_{12}$, and the MS operator H_{MS} includes the leading term of normal and specific mass shift (NMS, SMS) operators,

$$H_{\text{MS}} = H_{\text{NMS}} + H_{\text{SMS}} = \sum_{i=1}^{2}\frac{\boldsymbol{p}_i^2}{2m_0} + \frac{\boldsymbol{p}_1 \cdot \boldsymbol{p}_2}{m_0}, \tag{2}$$

where $m_0 = 7294.299\,536\,1 m_e$ and $m_0 = 5495.885\,275\,4 m_e$ [23] are the nuclear mass for ^{4}He and ^{3}He, respectively. The wave function $\psi(JM_J)$ for a state with angular momentum (J, M_J) is expanded as a linear combination of the configuration-state wave functions $\phi_{ij}(JM_J)$, which are constructed by the single-electron wave functions [21]. Using the Notre Dame basis sets [24,25] of B-spline functions, the single-electron wave functions are obtained by solving the single-electron Dirac equation.

The nonrelativistic Hamiltonian for the infinite nuclear mass of helium is solved with the Hylleraas-B-spline basis set [22],

$$\phi_{ij\ell_1\ell_2}(LM_L) = B_i^k(r_1)B_j^k(r_2)r_{12}^c Y_{\ell_1\ell_2}^{LM_L}(\hat{r}_1, \hat{r}_2) \pm \text{exchange}, \tag{3}$$

where L and M_L are the total orbital and magnetic quantum numbers, respectively, $Y_{\ell_1\ell_2}^{LM_L}(\hat{r}_1, \hat{r}_2)$ is the coupled spherical harmonic function, and $c = 0\,,1$.

The dynamic dipole polarizability of the magnetic sublevel $|N_g J_g M_{J_g}\rangle$ under linear polarized light with laser frequency ω is

$$\alpha_1(\omega) = \alpha_1^S(\omega) + \frac{3M_{J_g}^2 - J_g(J_g+1)}{J_g(2J_g-1)}\alpha_1^T(\omega), \tag{4}$$

where $\alpha_1^S(\omega)$ and $\alpha_1^T(\omega)$ are the scalar and tensor dipole polarizabilities, respectively, which can be expressed as the summation over all intermediate states,

$$\alpha_1^S(\omega) = \sum_{n \neq g}\frac{f_{gn}^{(1)}}{(\Delta E_{gn})^2 - \omega^2}, \tag{5}$$

$$\alpha_1^T(\omega) = \sum_{n \neq g}(-1)^{J_g+J_n}\sqrt{\frac{30(2J_g+1)J_g(2J_g-1)}{(2J_g+3)(J_g+1)}} \times \begin{Bmatrix} 1 & 1 & 2 \\ J_g & J_g & J_n \end{Bmatrix}\frac{f_{gn}^{(1)}}{(\Delta E_{gn})^2 - \omega^2}, \tag{6}$$

with $f_{gn}^{(1)}$ the dipole oscillator strength,

$$f_{gn}^{(1)} = \frac{2|\langle N_g J_g \| T_1 \| N_n J_n \rangle|^2 \Delta E_{gn}}{3(2J_g+1)}, \tag{7}$$

where $\Delta E_{gn} = E_n - E_g$ is the transition energy between the initial state $|N_g J_g\rangle$ and the intermediate state $|N_n J_n\rangle$, and T_1 is the dipole transition operator. The nonrelativistic polarizabilities are obtained by replacing the quantum number J with L in Eqs. (4)–(7).

The QED corrections to dynamic dipole polarizabilities are calculated by the perturbation theory [26] using energies and wave functions obtained from the nonrelativistic configuration interaction method [27],

$$\delta\alpha_1^{\text{QED}}(\omega) = 2\left[\sum_n \frac{\langle g|T_1|n\rangle\langle n|T_1|g\rangle\langle g|\delta H_{\text{QED}}|g\rangle[(E_n - E_g)^2 + \omega^2]}{[(E_n - E_g)^2 - \omega^2]^2} - 2\sum_{nm}\frac{\langle g|T_1|n\rangle\langle n|T_1|m\rangle\langle m|\delta H_{\text{QED}}|g\rangle(E_n - E_g)}{[(E_n - E_g)^2 - \omega^2](E_m - E_g)} - \sum_{nm}\frac{\langle g|T_1|n\rangle\langle n|\delta H_{\text{QED}}|m\rangle\langle m|T_1|g\rangle[(E_n - E_g)(E_m - E_g) + \omega^2]}{[(E_n - E_g)^2 - \omega^2][(E_m - E_g)^2 - \omega^2]}\right], \tag{8}$$

where $|g\rangle$ is the initial state, $|n\rangle$ and $|m\rangle$ represent intermediate states, and δH_{QED} is the QED operator. The expansion of δH_{QED} [28] to the leading order of α^3 is adopted in this work:

$$H_{\text{QED}}^{(3)} \simeq \frac{4Z\alpha^3}{3}\left\{\frac{19}{30} + \ln\left[(Z\alpha)^{-2}\right] - \ln\left(\frac{k_0}{Z^2}\right)\right\}[\delta^3(\mathbf{r}_1) + \delta^3(\mathbf{r}_2)] + O(\mathbf{r}_{12}), \tag{9}$$

where $\ln k_0$ is the Bethe logarithm, and $O(\mathbf{r}_{12})$ represents the remaining term connected with $\mathbf{r}_{12}$. We use $\ln k_0 = 4.364\,036\,82(1)$ and $4.366\,412\,72(7)$ [29] for the $2\,^3S_1$ and $2\,^1S_0$ states, respectively. $O(\mathbf{r}_{12})$ contributes -5.2×10^{-8} a.u. and -5.6×10^{-9} a.u. to the energies of $2\,^1S_0$ and $2\,^3S_1$ states of helium, respectively, which is three and four orders of magnitude smaller than 1.66×10^{-5} a.u. and 1.67×10^{-5} a.u. from the first term of Eq. (9). So in this work, the QED correction to the magic wavelengths is calculated by omitting the $O(\mathbf{r}_{12})$ contributions.

The nonrelativistic dynamic hyperpolarizability for the S state is

$$\gamma_0(\omega) = \frac{128\pi^2}{3}\left[\frac{1}{9}\mathcal{T}(1, 0, 1, \omega) + \frac{2}{45}\mathcal{T}(1, 2, 1, \omega)\right], \tag{10}$$

where $\mathcal{T}(L_a, L_b, L_c, \omega)$ is written as

$$\begin{aligned}\mathcal{T}(L_a, L_b, L_c, \omega) = {} & \sum_{mnk} \frac{\langle N_g L_g \| T_1 \| m L_a\rangle \langle m L_a \| T_1 \| n L_b\rangle \langle n L_b \| T_1 \| k L_c\rangle \langle k L_c \| T_1 \| N_g L_g\rangle}{(\Delta E_{mg} - \omega)\Delta E_{ng}(\Delta E_{kg} - \omega)} \\ & - \delta_{L_b,L_g} \sum_m \frac{|\langle N_g L_g \| T_1 \| m L_a\rangle|^2}{(\Delta E_{mg} - \omega)} \sum_k \frac{|\langle N_g L_g \| T_1 \| k L_c\rangle|^2}{(\Delta E_{kg} - \omega)^2}.\end{aligned} \tag{11}$$

Compared with the dynamic dipole polarizabilities, the accurate calculation of the dynamic hyperpolarizabilities is much more challenging, since the formula involves three summations over different intermediated states, which means the calculation of hyperpolarizability depends on the completeness of the energy spectrum of more intermediate states.

The magic wavelengths of the $2\,^3S \rightarrow 2\,^1S$ transition are determined from making the dynamic dipole polarizabilities of the $2\,^1S_0$ and $2\,^3S_1$ states equally. The accuracy of magic wavelengths depends on accurate energies and wave functions of initial and intermediate states. The high-precision B-spline RCI method was very successful in accurate calculation of atomic polarizabilities for the triplet $2\,^3S_1$ state of helium [21]. However, for the magic wavelengths around 320 nm of interest in the present work, it's clearly seen from Fig. 1, they are located at the edge of the $2\,^1S_0 \rightarrow 10\,^1P_1$, $2\,^1S_0 \rightarrow 11\,^1P_1$, and $2\,^1S_0 \rightarrow 12\,^1P_1$ resonance transitions. The accurate determination of these magic wavelengths requires construction of sufficient configurations in an appropriate box size to make sure that all transition energies from the $2\,^1S_0$ state to the $10\,^1P_1$, $11\,^1P_1$, and $12\,^1P_1$ Rydberg states are accurate. This is a biggest challenge for our RCI calculation.

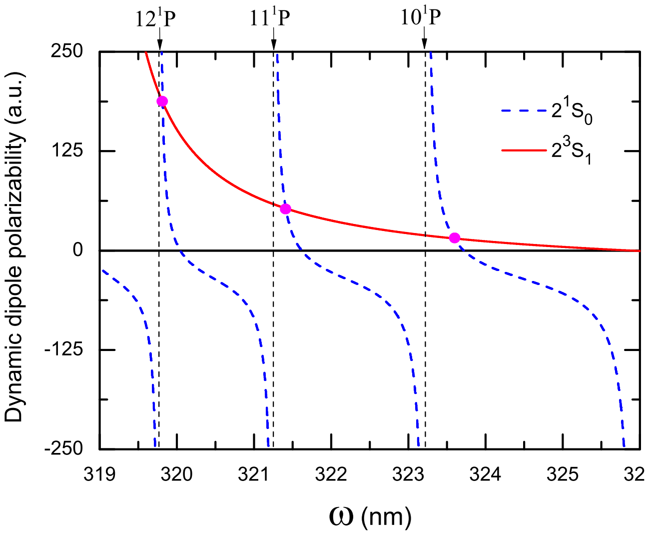

FIG. 1. Dynamic dipole polarizabilities (in a.u.) of helium for the photon energy 319 nm $\leqslant \omega \leqslant$ 326 nm. The solid red line and the dashed blue line represent the dynamic polarizabilities for $2\,^3S_1(M_J = \pm 1)$ and $2\,^1S_0$ states, respectively. The crossing points marked as a solid magenta circle are the magic wavelengths. The vertical lines are the resonance transition positions, and the black line denotes a horizontal line.

We optimize our RCI program by using OpenMP parallel and block calculations, which overcomes the problem of time-consuming and large memory required in calculating the electron-electron Coulomb and Breit interaction integrals. Extensive tests of the numerical stability for energies, matrix elements, polarizabilities, and magic wavelengths of helium are carried out.

In order to get accurate energies for the intermediate $n\,^1P_1 (n = 10\text{–}13)$ states, we fix the box size $R_0 = 600$ a.u. and increase the numbers of partial-wave $l_{\max}$, and B-spline basis sets N to test the convergence of energies. Seen from the Table I, when fixing $N = 50$ to increase $\ell_{\max}$, we get the converged energy of $-2.003\ 297\ 06(1)$ a.u. for the $12\,^1P_1$ state, which has eight significant digits.

For other $n\,^1P_1$ states, seen from Table II, all the energies for $n\,^1P_1 (n \leqslant 13)$ intermediate states have eight significant digits. That means the energy accuracy for all the states, even for the Rydberg states, can be guaranteed to the same level of precision from one diagonalization in the present RCI calculations. The Hylleraas energies [30] of Table II are derived by combining the values in Tables 11.7 and 11.8 of Ref. [30] and the ground-state energy of $-1.999\,832\,572\,508$ a.u. of He$^+$. Compared with the Hylleraas energies [30], which include

TABLE I. Energy (in a.u.) test of the $2\,^1S_0$ and $12\,^1P_1$ states of ^{4}He. N is the number of B spline, R_0 is the box size, and $\ell_{\max}$ presents the number of partial wave.

	$2\,^1S_0$		$12\,^1P_1$
$\ell_{\max}$	(N, R_0)=(45,100)	(N, R_0)=(50,600)	(N, R_0)=(50,600)
7	−2.145 783 68	−2.145 782 91	−2.003 297 046
8	−2.145 784 58	−2.145 783 74	−2.003 297 053
9	−2.145 785 15	−2.145 784 25	−2.003 297 057
10	−2.145 785 53	−2.145 784 58	−2.003 297 059
15	−2.145 786 27	−2.145 785 21	−2.003 297 063
Extrap.	−2.145 786(1)	−2.145 785(1)	−2.003 297 06(1)

TABLE II. Comparison of present RCI energies (in a.u.) for some selective $n\,^1P_1(n \leqslant 13)$ states of ^{4}He and ^{3}He. The numbers in parentheses are computational uncertainties.

	^{4}He	
State	RCI	Hylleraas [30]
$2\,^1P_1$	−2.123 650 17(2)	−2.123 654 51
$3\,^1P_1$	−2.054 968 56(2)	−2.054 970 17
$4\,^1P_1$	−2.030 896 59(2)	−2.030 897 47
$5\,^1P_1$	−2.019 734 98(2)	−2.019 735 59
$6\,^1P_1$	−2.013 664 02(2)	−2.013 664 52
$7\,^1P_1$	−2.009 999 98(2)	−2.010 000 41
$8\,^1P_1$	−2.007 620 18(2)	−2.007 620 57
$9\,^1P_1$	−2.005 987 70(2)	−2.005 988 07
$10\,^1P_1$	−2.004 819 48(2)	−2.004 819 84
$11\,^1P_1$	−2.003 954 83(2)	
$12\,^1P_1$	−2.003 297 06(1)	
$13\,^1P_1$	−2.002 784 91(4)	
	^{3}He	
State	RCI	Hylleraas [30]
$2\,^1P_1$	−2.123 552 83(2)	−2.123 557 20
$3\,^1P_1$	−2.054 875 71(2)	−2.054 877 36
$4\,^1P_1$	−2.030 805 19(2)	−2.030 806 11
$5\,^1P_1$	−2.019 644 21(2)	−2.019 644 86
$6\,^1P_1$	−2.013 573 59(2)	−2.013 574 20
$7\,^1P_1$	−2.009 909 74(2)	−2.009 910 20
$8\,^1P_1$	−2.007 530 06(2)	−2.007 530 50
$9\,^1P_1$	−2.005 897 67(2)	−2.005 898 08
$10\,^1P_1$	−2.004 729 51(2)	−2.004 729 91
$11\,^1P_1$	−2.003 864 90(2)	
$12\,^1P_1$	−2.003 207 09(4)	
$13\,^1P_1$	−2.002 695 04(4)	

TABLE III. Comparison of some reduced matrix elements between present RCI calculations and Hylleraas calculations [31] of the $2\,^1S_0 \rightarrow n\,^1P_1(n \leqslant 13)$ transitions for ^{4}He and ^{3}He. The numbers in parentheses are computational uncertainties.

	RCI		Hylleraas [31]
$2\,^1S_0 \rightarrow n\,^1P_1$	^{3}He	^{4}He	^{4}He
2	5.052 46(2)	5.052 06(8)	5.050 977
3	1.580 76(2)	1.580 81(2)	1.581 082
4	0.801 02(2)	0.801 03(2)	0.801 106
5	0.515 54(2)	0.515 53(2)	0.515 578
6	0.371 14(2)	0.371 14(2)	0.371 159
7	0.285 12(2)	0.285 12(2)	0.285 131
8	0.228 58(2)	0.228 58(2)	0.228 590
9	0.188 89(2)	0.188 89(2)	0.188 899
10	0.159 68(2)	0.159 67(2)	0.159 686
11	0.137 40(2)	0.137 39(2)	
12	0.119 92(2)	0.119 92(2)	
13	0.105 90(2)	0.105 89(2)	

the finite nuclear mass, relativistic, and anomalous magnetic moment corrections, our RCI energies are in good agreement with Hylleraas energies [30].

But for the energy of the $2\,^1S_0$ state, seen from Table I, since the electron-electron correlation is much larger than the $12\,^1P_1$ state, we cannot get eight significant digits from the present largest-scale RCI calculation. Even we decrease the box size R_0 to 100 a.u. and fix $N = 45$ to increase $\ell_{\max} = 15$, the convergent energy is −2.145 786(1) a.u., which is less accurate than the $n\,^1P_1(n \leqslant 13)$ states by one order of magnitude, and just has seven same digits compared with the best value of −2.145 786 909 a.u. [28]. So in the later determination of magic wavelengths, we replace our RCI energies of the $2\,^1S_0$ state of helium with the values of Ref. [28].

Table III gives a comparison of the reduced matrix elements for the dipole allowed $2\,^1S_0 \rightarrow n\,^1P_1(n \leqslant 13)$ transitions. The Hylleraas values [31] include the finite nuclear mass and the leading relativistic corrections. Compared with the Hylleraas values, present RCI results have four same digits for the $2\,^1S_0 \rightarrow n\,^1P_1(n \geqslant 5)$ transitions. The energies of $n\,^1S_0$, $n\,^3S_1$, and $n\,^3P_J$ states, and the reduced matrix elements for $2\,^1S_0 \rightarrow n\,^3P_1$, $2\,^3S_1 \rightarrow n\,^3P_J$, and $2\,^3S_1 \rightarrow n\,^1P_1$ transitions with $n \leqslant 13$ for ^{3}He and ^{4}He are presented in the Supplemental Material [32].

Since the 319.8 nm magic wavelength was proposed to trap helium for high-precision measurement, Table IV lists the convergent test for this particular magic wavelength of the $2\,^3S_1(M_J = \pm 1) \rightarrow 2\,^1S_0$ transition of ^{4}He. The corresponding dynamic dipole polarizabilities at the magic wavelengths are also listed. It is seen that both the parameters, N and $\ell_{\max}$, affect the convergent rate of numerical values. According to the values in the last three lines, we can obtain the extrapolated value of 319.814 3(4) nm for the magic wavelength. In order to take into account the incompleteness of configurations, the uncertainty of 319.814 3(4) nm is obtained by doubling the difference of 319.814 300 and 319.814 128 nm for the sake of conservativeness. Similarly, we can get the extrapolated polarizability of 186.96(6) a.u., which is more accurate than the semiempirical result of 189.3 a.u. [20].

For the ^{3}He atom, in Table V, the convergence tests of the 319.8 nm magic wavelength with and without the hyperfine

TABLE IV. Convergence test of 319.8 nm magic wavelength for the $2\,^3S_1(M_J = \pm 1) \rightarrow 2\,^1S_0$ transition of ^{4}He as the number of B splines, N increased with the number of the partial wave, $\ell_{\max} = 7$, and as $\ell_{\max}$ increased with $N = 50$ by choosing the box size, $R_0 =$ 600 a.u. The convergence test for the dynamic dipole polarizabilities at the corresponding magic wavelengths are also listed.

	$\ell_{\max}$=7	
N	λ_m	$\alpha_1(\omega)$
40	319.828 217	183.903 70
45	319.815 649	186.660 50
50	319.814 254	186.967 81
55	319.814 140	186.992 26
60	319.814 128	186.995 32
$\ell_{\max}$	N=50	
10	319.814 287	186.959 58
15	319.814 299	186.957 01
20	319.814 300	186.956 61
Extrap.	319.814 3(4)	186.96(6)

TABLE V. Convergence test of 319.8 nm magic wavelength for the $2\,^3S_1(M_J=\pm1)\to 2\,^1S_0$ transition and the $2\,^3S_1(F=\frac{3}{2}, M_F=\frac{3}{2})\to 2\,^1S_0(F=\frac{1}{2}, M_F=\frac{1}{2})$ hyperfine transition of ^{3}He as the number of B splines, N, increased by fixing the number of the partial wave as $\ell_{\max}=7$ and choosing the box size as $R_0=600$ a.u. The dynamic dipole polarizabilities at the corresponding magic wavelengths are also listed.

	$2\,^3S_1(M_J=\pm1)$ $\to 2\,^1S_0$		$2\,^3S_1(F=\frac{3}{2}, M_F=\frac{3}{2})$ $\to 2\,^1S_0(F=\frac{1}{2}, M_F=\frac{1}{2})$	
N	λ_m	$\alpha_1(\omega)$	λ_m	$\alpha_1(\omega)$
40	319.843 338	184.136 47	319.843 372	183.888 81
45	319.830 791	186.897 83	319.830 832	186.641 95
50	319.829 394	187.201 98	319.829 437	186.945 04
55	319.829 278	187.237 65	319.829 320	186.980 95
60	319.829 266	187.232 93	319.829 308	186.976 20
Extrap.	319.829 2(4)	187.22(6)	319.829 3(4)	186.96(6)

effect are presented. For the $2\,^3S_1(M_J=\pm1)\to 2\,^1S_0$ transition, the extrapolated values of 319.829 2(4) nm and 187.22(6) a.u. are, respectively, for the magic wavelength and the corresponding dynamic dipole polarizability. For the $2\,^3S_1(F=\frac{3}{2}, M_F=\frac{3}{2})\to 2\,^1S_0(F=\frac{1}{2}, M_F=\frac{1}{2})$ hyperfine transition, we use the hyperfine energy shifts of Ref. [33] for the $2\,^1S_0$, $2\,^3S_1$, and $n\,^{1,3}P_J(n\leqslant 10)$ states. For higher $n\,^{1,3}P_J$ intermediate states, the hyperfine energy shifts are obtained by fitting the hyperfine splitting of $n\,^{1,3}P_J(n\leqslant 10)$ states. The reduced matrix elements between hyperfine levels can be transformed by the Eq. (4) of Ref. [34]. Then we replace the hyperfine energies and matrix elements into Eqs. (4)–(7) to get dynamic dipole polarizabilities for extracting the magic wavelengths. We find that the hyperfine effect has large correction to $\alpha_1(\omega)$, but only increases about 0.1 pm on the extrapolated λ_m of 319.829 2(4) nm, which can be taken as one source of the uncertainty in the final recommended magic wavelength.

In addition, the QED corrections to all the magic wavelengths are extracted by performing the calculation of QED correction to the dynamic dipole polarizabilities. The values are listed in the Table VI. Especially for the 319.8 nm magic wavelength, leading order of QED correction is 0.001 00(2) nm. Other terms, such as the second derivative of the Bethe logarithm, Araki-Sucher term, and high-order QED corrections, would bring possible sources of the error. For the sake of conservativeness, we can multiply the uncertainty by 10. So the final QED correction of 0.0010(2) nm is indicated to the 319.8 nm magic wavelength, which can be added into present RCI values, then we can get the recommended magic wavelengths of 319.815 3(6) and 319.815 4(6) nm, respectively, for the $2\,^3S_1(M_J=\pm1)\to 2\,^1S_0$ and $2\,^3S_1(M_J=0)\to 2\,^1S_0$ transitions of ^{4}He. Similarly, with the QED and hyperfine structure corrections taken into account for ^{3}He, we can give the recommended values of 319.830 2(7) and 319.830 4(7) nm, respectively, for the $2\,^3S_1(M_J=\pm1)\to 2\,^1S_0$ and $2\,^3S_1(M_J=0)\to 2\,^1S_0$ transitions of ^{3}He. Our recommended value of 319.815 3(6) nm for ^{4}He agrees well with recent measurement results of 319.815 92(15) nm [35]. And the present magic wavelength of ^{3}He would provide theoretical reference for designing ODT experiments to help resolve the nuclear radius discrepancy of helium isotopes.

Except the important application of the 319.8 nm magic wavelength of helium, both the 321.4 and 323.5 nm magic wavelengths can also be used to design experiments once a high-power laser can be realized. The magic wavelengths obtained from present RCI calculations are 323.587 9(4) and 321.409 5(4) nm for the $2\,^3S_1(M_J=\pm1)\to 2\,^1S_0$ transition of ^{4}He. Taking the QED correction into account, we recommend 323.588 9(6) and 321.410 5(6) nm as the final values of magic wavelengths. Similarly, for the $2\,^3S_1(M_J=\pm1)\to 2\,^1S_0$ transition of ^{3}He, with the QED and hyperfine corrections included, the magic wavelengths of 323.604 1(7) and 321.425 7(7) nm are recommended.

Table VI summarizes the first nine magic wavelengths in the range of 318–413 nm from two independent calculations of the Hyllerass-B-splines and RCI methods. All the values from two different theoretical methods are consistent. The relativistic and finite nuclear mass corrections on all the magic wavelengths are less than 60 pm. For the RCI calculation, the difference of all the magic wavelengths between ^{4}He and ^{3}He

TABLE VI. The first nine magic wavelengths (in nm) of the $2\,^3S_1\to 2\,^1S_0$ transition of helium. The numbers in parentheses are computational uncertainties. The uncertainties in the present RCI values evaluated from the incompleteness of configuration space. The values of QED correction only represents the convergence results of our numerical calculation; the uncertainty would be multiplied by 10 in the final QED correction for conservativeness.

	Hyllerass B splines	RCI					Ref. [20]	
	$2\,^3S\to 2\,^1S$	$2\,^3S_1(M_J=\pm1)\to 2\,^1S_0$		$2\,^3S_1(M_J=0)\to 2\,^1S_0$		QED	$2\,^3S_1\to 2\,^1S_0$	
No.	$^\infty$He	^{4}He	^{3}He	^{4}He	^{3}He	$2\,^3S_1\to 2\,^1S_0$	^{4}He	^{3}He
1	412.16(2)	412.167(5)	412.166(5)	412.173(8)	412.177(7)	− 0.000 43(2)	411.863	
2	352.299(4)	352.335(3)	352.351(4)	352.336(3)	352.352(4)	0.001 12(2)	352.242	
3	338.641(2)	338.681 7(5)	338.697 2(5)	338.681 8(5)	338.697 4(5)	0.001 07(2)	338.644	
4	331.240(1)	331.282 7(4)	331.298 1(4)	331.282 8(4)	331.298 3(4)	0.001 04(2)	331.268	
5	326.633(1)	326.677 0(4)	326.692 2(4)	326.677 1(4)	326.692 3(4)	0.001 03(2)	326.672	
6	323.544(1)	323.587 9(4)	323.603 1(4)	323.588 0(4)	323.603 4(4)	0.001 02(2)	323.587	323.602
7	321.366(1)	321.409 5(4)	321.424 7(4)	321.409 6(4)	321.424 9(4)	0.001 01(2)	321.409	321.423
8	319.771(1)	319.814 3(4)	319.829 2(4)	319.814 4(4)	319.829 4(4)	0.001 00(2)	319.815	319.830
9	318.567(1)	318.610 5(8)	318.625 6(8)	318.610 6(8)	318.625 8(8)	0.001 11(2)	318.611	318.626

TABLE VII. Dynamic hyperpolarizabilities (in a.u.) at the nine magic wavelengths for the $2\,^1S$ and $2\,^3S$ states of $^\infty$He. The high-order ac Stark shifts (in Hz) are also presented in the last column. The electric field intensity $F \approx 1.58 \times 10^{-7}$ a.u. is evaluated from real experimental condition [35]. The numbers in the square brackets denote powers of ten. The numbers in parentheses are computational uncertainties.

No.	$2\,^1S$	$2\,^3S$	$\frac{1}{24}\Delta\gamma_0(\omega)F^4$
1	−6(4)[6]	−2.3(5)[8]	−3.9[−5]
2	−1.2(1)[6]	−3.6(9)[7]	−6.0[−6]
3	−4.1(9)[6]	−2.4(9)[7]	−3.4[−6]
4	−1.5(7)[7]	−3.7(8)[7]	−3.6[−6]
5	−2.9(4)[7]	−5.7(6)[7]	−4.8[−6]
6	−9.6(2)[7]	−1.1(3)[8]	−2.6[−6]
7	−5.4(1)[8]	−3.7(3)[8]	3.1[−5]
8	−1.0(1)[10]	−3.4(1)[9]	1.2[−3]
9	4.2(1)[11]	3.9(1)[10]	−6.6[−2]

are less than 17 pm. It's noticed that the QED corrections listed in the Table VI only represent the convergence results of present numerical calculation, the uncertainty may be multiplied by 10 in the final QED correction for conservatively taking other neglected contributions into account.

Table VII presents the dynamic hyperpolarizabilities at the nine magic wavelengths of Table VI for the $2\,^1S$ and $2\,^3S$ states of $^\infty$He by using the Hyllerass-B-splines method. And the high-order Ac Stark shift at each magic wavelength is also estimated. Especially, for the 319.8 nm magic wavelength, the dynamic hyperpolarizabilities are -1.0×10^{10} a.u. and -3.4×10^9 a.u. for the $2\,^1S$ and $2\,^3S$ states of $^\infty$He, respectively. The difference of the dynamic hyperpolarizabilities for the $2\,^3S \rightarrow 2\,^1S$ transition is $\Delta\gamma_0(\omega) = 6.7 \times 10^9$ a.u. If the power of the incident trapping laser beam is $P = 0.2\,W$ with beam waist $w_0 = 85\,\mu m$, then we can get the electric field intensity $F \approx 1.58 \times 10^{-7}$ a.u. Accordingly, the higher-order Ac Stark shift is evaluated as $\frac{1}{24}\Delta\gamma_0(\omega)F^4 \approx 1.7 \times 10^{-19}$ a.u. $\approx$1.2 mHz, it is smaller by six orders of magnitude than the 1.8 kHz uncertainty of the absolute frequency for the $2\,^3S_1 \rightarrow 2\,^1S_0$ transition of ^{4}He [7], which indicates the high-order Ac Stark shift can be neglected for the precision spectroscopy measurement of the $2\,^3S_1 \rightarrow 2\,^1S_0$ transition of helium by implementation of a magic wavelength trap.

In summary, the improved RCI method enables us to calculate the dynamic dipole polarizabilities in a wide range of laser frequency for both $2\,^3S_1$ and $2\,^1S_0$ states of helium. A series of magic wavelengths for the $2\,^3S_1 \rightarrow 2\,^1S_0$ forbidden transition of ^{4}He and ^{3}He are accurately determined. The nonrelativistic calculations of magic wavelength for $^\infty$He are also carried out by using the Hylleraas-B-spline method. Further, the leading order of QED corrections on the magic wavelengths have been taken into account. For ^{3}He, the correction from hyperfine structure to the magic wavelengths has been calculated. In addition, the high-order ac Stark shifts related with the dynamic hyperpolarizabilities are estimated. All the magic wavelengths from two different theoretical methods are consistent. The present recommended magic wavelength of 319.815 3(6) nm for ^{4}He is in good agreement with the high-precision measurement value of 319.815 92(15) nm [35]. The present magic wavelength of 319.830 2(7) nm for ^{3}He provides an important reference for experimental design of a magic wavelength trap to eliminate the ac Stark shift for the precision spectroscopy of the $2\,^3S_1 \rightarrow 2\,^1S_0$ transition of helium in the future.

We thank Wim Vassen for the early suggestion to carry out this work. We also thank Yong-Bo Tang for his discussion on the improvement of the present RCI program. This work was supported by the Strategic Priority Research Program of the Chinese Academy of Sciences under Grants No. XDB21010400 and No. XDB21030300, by the National Key Research and Development Program of China under Grant No. 2017YFA0304402, and by the National Natural Science Foundation of China under Grants No. 11474319, No. 11704398, No. 11774386, No. 91536102, and No. 11674253.

---

[1] R. Pohl, A. Antognini, F. Nez, F. D. Amaro, F. Biraben, J. M. R. Cardoso, D. S. Covita, A. Dax, S. Dhawan, L. M. P. Fernandes *et al.*, Nature **466**, 213 (2010).

[2] A. Antognini, F. Nez, K. Schuhmann, F. D. Amaro, F. Biraben, J. M. R. Cardoso, D. S. Covita, A. Dax, S. Dhawan, M. Diepold *et al.*, Science **339**, 417 (2013).

[3] P. J. Mohr, D. B. Newell, and B. N. Taylor, Rev. Mod. Phys. **88**, 035009 (2016).

[4] A. Beyer, L. Maisenbacher, A. Matveev, R. Pohl, K. Khabarova, A. Grinin, D. C. Yost, T. W. Hänsch, N. Kolachevsky, and T. Udem, Science **358**, 79 (2017).

[5] J. N. Tan, S. M. Brewer, and N. D. Guise, Phys. Scr. **2011**, 014009 (2011).

[6] A. Antognini, F. Biraben, J. M. R. Cardoso, D. S. Covita, A. Dax, L. M. P. Fernandes, A. L. Gouvea, T. W. Hänsch, M. Hildebrandt, and P. Indelicato, Can. J. Phys. **89**, 47 (2011).

[7] R. van Rooij, J. S. Borbely, J. Simonet, M. D. Hoogerland, K. S. E. Eikema, R. A. Rozendaal, and W. Vassen, Science **333**, 196 (2011).

[8] K. A. H. van Leeuwen and W. Vassen, Europhys. Lett. **76**, 409 (2006).

[9] D. Shiner, R. Dixson, and V. Vedantham, Phys. Rev. Lett. **74**, 3553 (1995).

[10] D. C. Morton, Q. Wu, and G. W. F. Drake, Phys. Rev. A **73**, 034502 (2006).

[11] P. C. Pastor, G. Giusfredi, P. DeNatale, G. Hagel, C. de Mauro, and M. Inguscio, Phys. Rev. Lett. **92**, 023001 (2004).

[12] P. Cancio Pastor, L. Consolino, G. Giusfredi, P. De Natale, M. Inguscio, V. A. Yerokhin, and K. Pachucki, Phys. Rev. Lett. **108**, 143001 (2012).

[13] K. Pachucki and V. A. Yerokhin, J. Phys. Chem. Ref. Data **44**, 031206 (2015).

[14] V. Patkóš, V. A. Yerokhin, and K. Pachucki, Phys. Rev. A **94**, 052508 (2016).

[15] V. Patkóš, V. A. Yerokhin, and K. Pachucki, Phys. Rev. A **95**, 012508 (2017).

[16] X. Zheng, Y. R. Sun, J.-J. Chen, W. Jiang, K. Pachucki, and S.-M. Hu, Phys. Rev. Lett. **119**, 263002 (2017).

[17] P. C. Pastor, G. Giusfredi, P. De Natale, G. Hagel, C. de Mauro, and M. Inguscio, Phys. Rev. Lett. **97**, 139903(E) (2006).

[18] H. Kim, M. S. Heo, W. K. Lee, C. Y. Park, H. G. Hong, S. W. Hwang, and D. H. Yu, Jpn. J. Appl. Phys. **56**, 050302 (2017).

[19] S. L. Campbell, R. B. Hutson, G. E. Marti, A. Goban, N. Darkwah Oppong, R. L. McNally, L. Sonderhouse, J. M. Robinson, W. Zhang, B. J. Bloom *et al.*, Science **358**, 90 (2017).

[20] R. P. M. J. W. Notermans, R. J. Rengelink, K. A. H. van Leeuwen, and W. Vassen, Phys. Rev. A **90**, 052508 (2014).

[21] Y.-H. Zhang, L.-Y. Tang, X.-Z. Zhang, and T.-Y. Shi, Phys. Rev. A **93**, 052516 (2016).

[22] S.-J. Yang, X.-S. Mei, T.-Y. Shi, and H.-X. Qiao, Phys. Rev. A **95**, 062505 (2017).

[23] P. J. Mohr, B. N. Taylor, and D. B. Newell, Rev. Mod. Phys. **84**, 1527 (2012).

[24] W. R. Johnson, S. A. Blundell, and J. Sapirstein, Phys. Rev. A **37**, 307 (1988).

[25] K. Beloy and A. Derevianko, Comput. Phys. Commun. **179**, 310 (2008).

[26] K. Pachucki and J. Sapirstein, Phys. Rev. A **63**, 012504 (2000).

[27] Y.-H. Zhang, L.-Y. Tang, X.-Z. Zhang, and T.-Y. Shi, Phys. Rev. A **92**, 012515 (2015).

[28] V. A. Yerokhin and K. Pachucki, Phys. Rev. A **81**, 022507 (2010).

[29] G. W. F. Drake and S. P. Goldman, Can. J. Phys. **77**, 835 (1999).

[30] G. W. F. Drake, *Handbook of Atomic, Molecular, and Optical Pphysics* (Springer, New York, 2006).

[31] G. W. F. Drake and D. C. Morton, Astrophys. J. Suppl. Ser. **170**, 251 (2007).

[32] See Supplemental Material at http://link.aps.org/supplemental/10.1103/PhysRevA.98.040501 for other energies and matrix elements of helium isotopes.

[33] D. C. Morton, Q. Wu, and G. W. F. Drake, Can. J. Phys. **84**, 83 (2006).

[34] J. Jiang and J. Mitroy, Phys. Rev. A **88**, 032505 (2013).

[35] R. J. Rengelink, Y. van der Werf, R. P. M. J. W. Notermans, R. Jannin, K. S. E. Eikema, M. D. Hoogerland, and W. Vassen, arXiv:1804.06693.